Genetically induced microtubule disruption in the mouse intestine impairs intracellular organization and transport

Andrew Muroyama, Michael Terwilliger, Bushu Dong, Harrison Suh, and Terry Lechler*
Departments of Dermatology and Cell Biology, Duke University, Durham, NC 27708

ABSTRACT **In most differentiated cells, microtubules reorganize into noncentrosomal arrays that are cell-type specific. In the columnar absorptive enterocytes of the intestine, microtubules form polarized apical–basal arrays that have been proposed to play multiple roles. However, in vivo testing of these hypotheses has been hampered by a lack of genetic tools to specifically perturb microtubules. Here we analyze mice in which microtubules are disrupted by conditional inducible expression of the microtubule-severing protein spastin. Spastin overexpression resulted in multiple cellular defects, including aberrations in nuclear and organelle positioning and deficient nutrient transport. However, cell shape, adhesion, and polarity remained intact, and mutant mice continued to thrive. Notably, the phenotypes of microtubule disruption are similar to those induced by microtubule disorganization upon loss of CAMSAP3/Nezha. These data demonstrate that enterocyte microtubules have important roles in organelle organization but are not essential for growth under homeostatic conditions.**

Monitoring Editor
Manuel Théry
CEA, Hopital Saint Louis

Received: Jan 24, 2018
Revised: Mar 29, 2018
Accepted: May 1, 2018

INTRODUCTION

The past two decades have provided significant insight into microtubule-binding proteins and their effects on microtubule dynamics and organization in cultured cells. The roles of microtubules, as well as their organization and dynamics, in intact tissues are less well-understood (Muroyama and Lechler, 2017a). In most differentiated cells, including the intestine, microtubules adopt noncentrosomal organizations, but we know little about how these networks form or their in vivo functions.

The intestinal epithelium is a highly proliferative and polarized tissue. Proliferation is restricted to crypts, which are invaginations of the epithelium into the underlying mesenchyme (Tan and Barker, 2014). Crypt cells give rise to differentiated enterocytes, goblet cells, and enteroendocrine cells that populate the villus. Enterocytes, the most abundant of these, are columnar epithelia with an essential role in nutrient digestion, absorption, and transport. Prior work on microtubule function within the intestinal epithelium relied on cultured cells, such as Caco-2, or drug treatment of intestinal explants (Hugon *et al.*, 1987; Achler *et al.*, 1989; Eilers *et al.*, 1989; Matter *et al.*, 1990; Gilbert *et al.*, 1991). It remains unclear whether the microtubule arrays formed in cultured cells fully recapitulate the normal in vivo architecture. Additionally, in vitro culture of intestinal explants may alter normal physiology, and drug treatment may induce nonspecific effects. These studies have revealed somewhat conflicting results on the role of microtubules in cell polarity and cell–cell adhesion formation. For example, whether microtubules are strictly required for maintenance of cell polarity remains controversial (Salas *et al.*, 1986; Cohen *et al.*, 2004; Noordstra *et al.*, 2016; Toya *et al.*, 2016). Importantly, neither of the aforementioned approaches allow for insights into roles for microtubules in physiology over extended time periods in an intact tissue.

More recently, gene ablation has been used to assess microtubule functions in vivo. For example, global loss of the CKK domain of CAMSAP3/Nezha, a minus-end anchoring protein, resulted in defects in microtubule organization in the intestine (Toya *et al.*, 2016). The mice failed to thrive, although it remains unclear whether this was a consequence of intestinal defects or alterations in other tissues. This raises the following questions: 1) Can additional functions for microtubules be uncovered by examining a complete loss of microtubules? 2) Are microtubules in differentiated intestinal cells

This article was published online ahead of print in MBoC in Press (http://www.molbiolcell.org/cgi/doi/10.1091/mbc.E18-01-0057) on May 9, 2018.

*Address correspondence to: Terry Lechler (terry.lechler@duke.edu).

Abbreviations used: γ-TuRC, gamma-tubulin ring complex; MDCK, Madin–Darby canine kidney; MTOC, microtubule-organizing center; PCM, pericentriolar material.

required for proper intestinal physiology? To answer these questions, it is necessary to disrupt microtubules rather than simply alter their organization.

We have taken advantage of a mouse line in which the microtubule-severing protein spastin is expressed in a doxycycline-dependent manner (Muroyama and Lechler, 2017b). Prior studies demonstrated that this is sufficient for microtubule disruption in other tissues in *Drosophila*, *Caenorhabditis elegans*, and mice (Sherwood *et al.*, 2004; Quintin *et al.*, 2016; Muroyama and Lechler, 2017b). Our strategy allowed us to induce long-term disruption of microtubules in the villus without affecting the proliferative cells of the crypt. In combination with a novel Nezha allele, which affords conditional deletion, we demonstrate that microtubule disorganization yields phenotypes consistent with microtubule disruption.

RESULTS AND DISCUSSION

Centrosome composition and microtubule organization in the intestinal epithelium

The intestinal epithelium is composed of two spatially segregated compartments, crypts and villi (Clevers, 2013; Tan and Barker, 2014). The crypt contains proliferative stem and transit-amplifying cells, along with differentiated Paneth cells. As cells exit the crypt and enter the villus, they terminally differentiate. We began by analyzing microtubule reorganization as cells differentiate along the crypt-villus axis. In crypts, microtubules were primarily aligned along the apical–basal axis of the cell, with a number of microtubule ends concentrated at the small apical surfaces of these cells (Figure 1A). A number of these microtubules extended along the lateral wall and appeared to continue along the basal surface (Figure 1B). Imaging of microtubules in isolated epithelial wholemounts confirmed the presence of an extensive basal microtubule network in crypt cells (Figure 1B). Similar networks have been reported in Madin–Darby canine kidney (MDCK) cells (Reilein *et al.*, 2005).

In villi, microtubules formed apical–basal arrays that were highly enriched on the apical side of the nucleus, with a few microtubules extending to the basal surface (Figure 1, C and D). This is consistent with previous reports in simple columnar epithelial cells (Troutt and Burnside, 1988; Bacallao *et al.*, 1989; Mogensen *et al.*, 1989; Toya and Takeichi, 2016). When viewed from the apical surface, an apical microtubule network is apparent, a feature that was recently described in Eph4 cells (Yano *et al.*, 2013). In villi we found no evidence for the basal networks found in crypts, either in tissue section or in epithelial wholemounts. Taking the results together, we conclude that microtubules undergo a striking reorganization as these cells progress through differentiation.

To better understand how differences in microtubule organization might be controlled, we examined the position and composition of centrosomes, which are microtubule-organizing centers (MTOCs) in most proliferative cell types. Centrin is a centriolar protein that marks all centrosomes in the intestinal epithelium. We found that it was concentrated in puncta at the apical region of crypt cells in the same region where microtubule density was highest (Figure 1, E and F). This is consistent with the centrosome acting as an MTOC in these cells, although the high density of microtubules makes direct observation of individual microtubules impossible with conventional light microscopy. In villi, all cells maintained centrin puncta on the apical side of the cell, demonstrating that differentiation does not induce loss of centrioles (Figure 1E). Notably, we did not observe enrichment of microtubules around the centrosomes in villi, demonstrating that centrosomes do not act as MTOCs in these differentiated cells (Figure 1F). Additionally, centrioles were not obligately attached to one another in villar cells and were randomly distributed in the *xy* plane of the cell when viewed from above (Figure 1, G and H).

Although centrioles were intact in all cells, we noted a striking reduction of pericentriolar material (PCM) between crypts and villi. CDK5RAP2, a pericentriolar protein that promotes γ-TuRC nucleation activity, was robustly associated with apical puncta in crypts. In contrast, villar cells had very low levels of CDK5RAP2 at centrosomes (Figure 1, I–K). Pericentrin showed a similar localization pattern, suggesting that the pericentriolar material is largely lost upon differentiation (Figure 1K). To test this, we examined two additional PCM proteins, γ-tubulin and Nedd1. In crypts, both Nedd1 and γ-tubulin were associated with apical puncta. These puncta colocalized with pericentrin, but both also had a diffuse apical localization in addition to their centrosomal localization. In villar cells, there was negligible Nedd1 and γ-tubulin associated with centrosomes. Instead, these proteins were found associated with the apical side of the cell. This relocalization of γ-tubulin has been noted before and is consistent with MTOC activity shifting from the centrosome to the apical cortex where microtubule minus ends are tethered (Salas, 1999). It is notable that Nedd1 demonstrates a similar reorganization as γ-TuRC because Nedd1/γ-TuRC complexes have been implicated in anchoring microtubule minus ends in keratinocytes (Muroyama *et al.*, 2016). Taking the results together, we demonstrate that microtubule organization and centrosome composition is altered upon differentiation in the intestinal epithelium, similar to findings in simple epithelia of lower organisms (Brodu *et al.*, 2010; Feldman and Priess, 2012).

Disruption of microtubules in differentiated cells of the intestinal epithelium

To test the functions of microtubules in differentiated intestinal cells, we generated Villin-rtTA; TRE-HA-spastin mice (referred to as Spastin^{Villi} mice; Figure 2A). This allows for doxycycline-inducible expression of the microtubule-severing protein spastin in villin-expressing cells. A similar approach was recently used to uncover novel roles for microtubules in the epidermis (Muroyama and Lechler, 2017b). In TRE-HA-spastin and in Spastin^{Villi} mice not treated with doxycycline, HA was not expressed (unpublished data). In contrast, upon doxycycline administration we saw robust HA staining throughout the intestinal villi, in more than 95% of cells (Figure 2, B and G). Critically, spastin was not induced in the crypts, which house the intestinal stem cells. Consistent with this, we did not see any mitotic phenotypes in this cell compartment; proliferation and apoptosis rates were normal (Supplemental Figure 1, A–C).

Some cell types are refractory to spastin-induced microtubule disassembly, potentially due to posttranslational modifications of tubulins (Sherwood *et al.*, 2004; Valenstein and Roll-Mecak, 2016). We therefore examined microtubules in Spastin^{Villi} mice and found robust loss of microtubules in the villi of these mice (Figure 2, D–F and H). Quantitation revealed an 80% loss of fluorescence intensity, with the remaining signal likely due to tubulin dimers and short filaments (Figure 2F). Similarly, staining for Glu-tubulin revealed a dramatic decrease in microtubules (Figure 2H). Surprisingly, this did not result in an overt gross phenotype even after 2 wk of doxycycline treatment (a time period over which the epithelium would have been replaced multiple times), and there was no change in animal weight (Figure 2C). This demonstrated the remarkable finding that microtubules in differentiated cells of the intestine were not required for viability under standard housing conditions. We next addressed whether there were consequences at the cellular and tissue level when microtubules were disrupted.

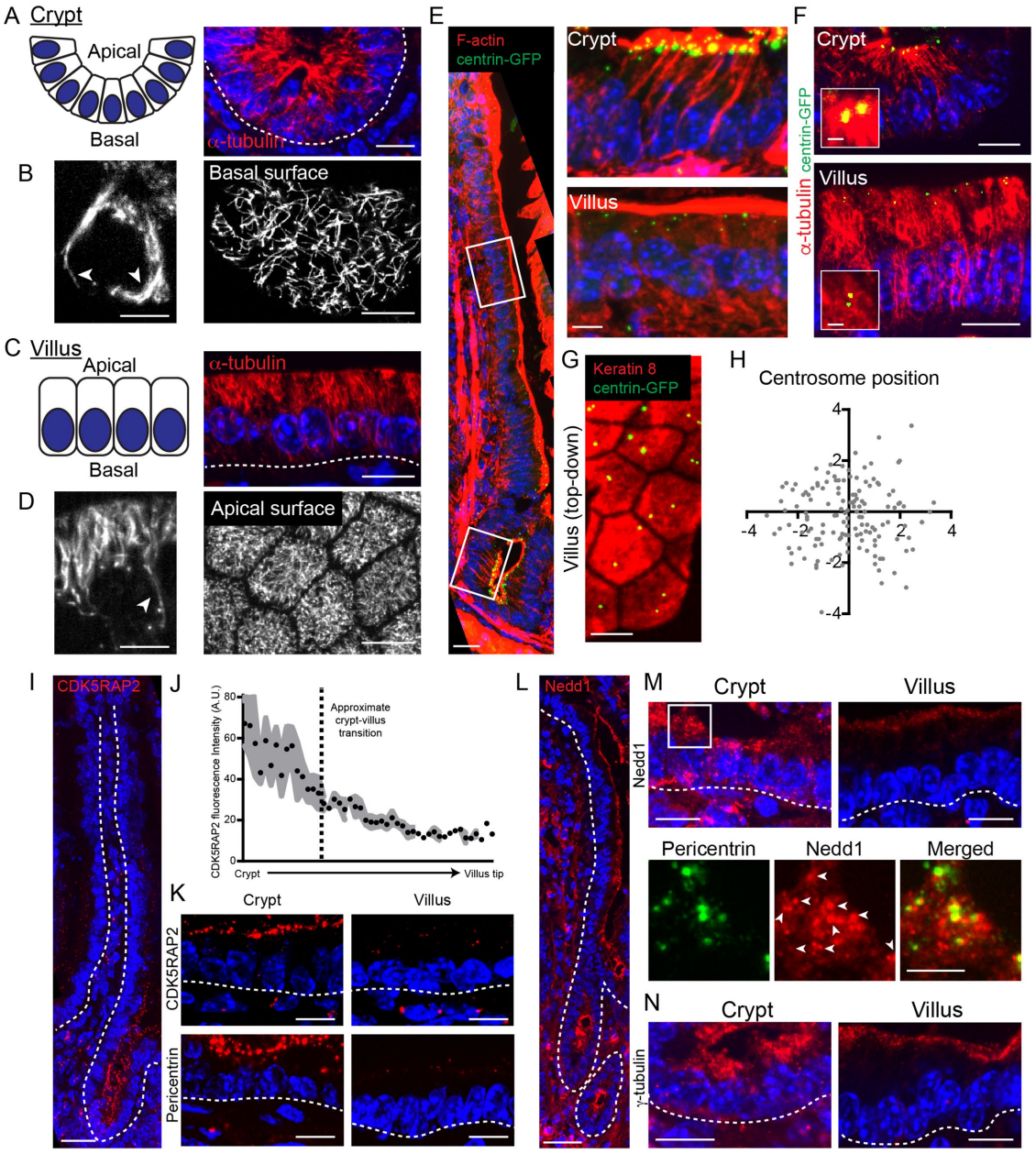

FIGURE 1: Microtubule and centrosome reorganization during intestinal differentiation. (A) Organization of crypt epithelium in cross-section. Corresponding cross-section showing microtubule organization in crypts. Scale = 10 μm. (B) Single optical section of a crypt cell. Scale = 5 μm. Arrows denote long microtubules growing along the basal surface. Single optical section of the basal surface of a crypt showing an elaborate microtubule network along the basal membrane. Scale = 10 μm. (C) Organization of villar epithelium in cross-section. Corresponding cross-section showing microtubule organization in villi. Scale = 10 μm. (D) Single optical section of cell in the villus. Scale = 5 μm. Arrow denotes a long microtubule that stops growing when it reaches the basal surface. Single top-down optical section showing a dense apical microtubule network in villar cells. Scale = 10 μm. (E) Stitched image of a single crypt-villus axis from a CMV-centrin-GFP mouse. Scale = 25 μm. Zoomed regions on the right show that the centrioles persist during intestinal differentiation. Scale = 5 μm. (F) Centriole position relative to microtubules in the crypt and villi. Scale = 10 μm. Scale for zoomed region = 1 μm. (G) Top-down view of a villus showing centriole position within the *xy* plane. Scale = 5 μm. (H) Mapping centriole position within the *xy* plane in villar cells. $n = 146$ centrosomes. (I) Stitched image of a single crypt-villus axis showing CDK5RAP2 localization. Scale = 25 μm. (J) Quantification of CDK5RAP2 fluorescence intensity along the crypt-villus axis. (K) CDK5RAP2 and pericentrin localization in the crypt and villar cells. Scale = 10 μm. (L) Stitched image of a single crypt-villus axis showing Nedd1 localization. Scale = 25 μm. (M) Nedd1 localization in the crypt and villus (top). Scale = 10 μm. Bottom panels show the zoomed region on the apical surface of the crypt, where Nedd1 is colocalized with pericentrin and also forms noncentrosomal clusters at the apical surface. White arrows indicate pericentrin foci. Scale = 5 μm. (N) γ-Tubulin localization in the intestinal crypt and villus. Scale = 10 μm. All dotted lines indicate basement membrane.

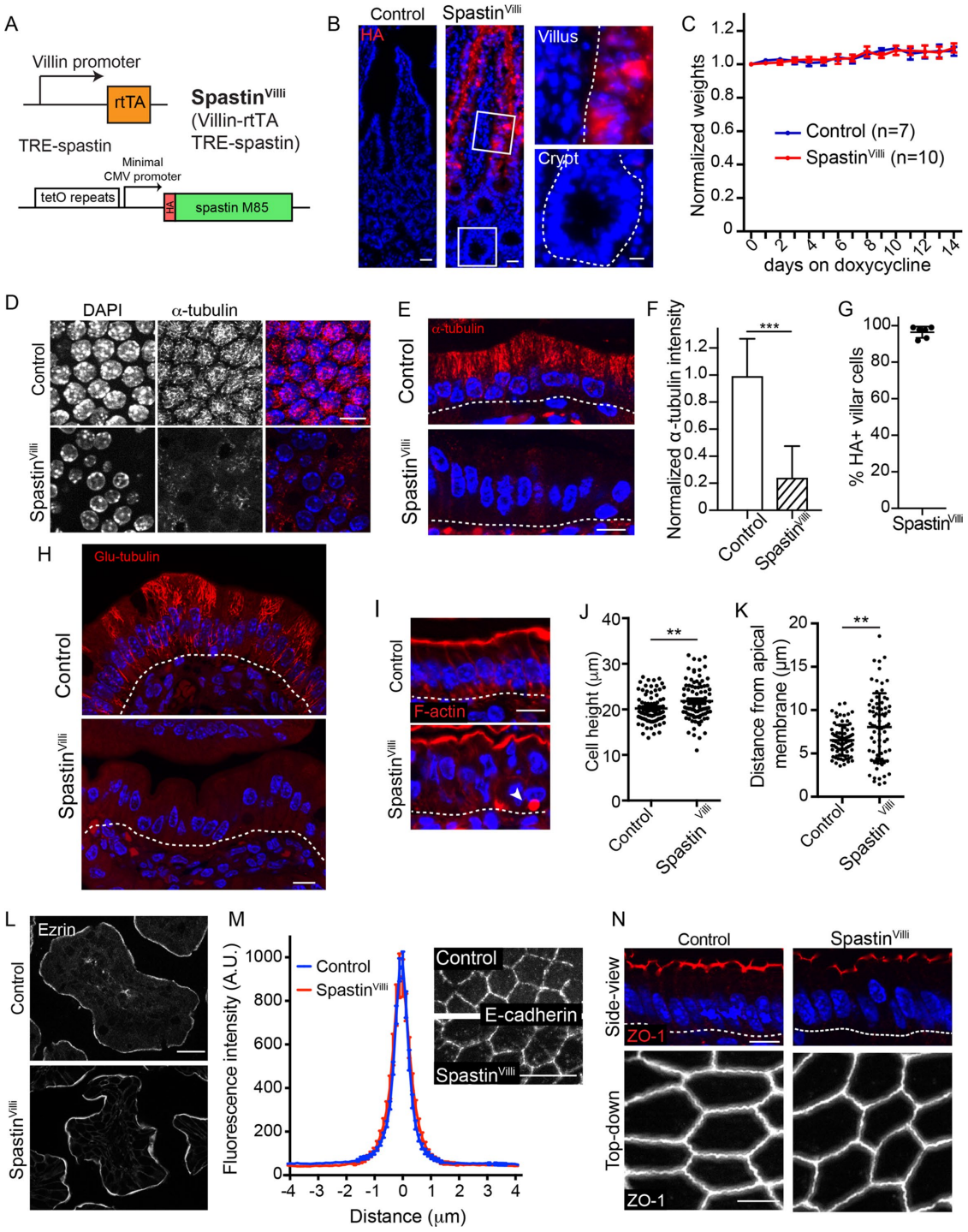

FIGURE 2: Effects of microtubule disruption in enterocytes. (A) Alleles used to generate Spastin^{Villi} mice. (B) HA-spastin expression after 48 h of doxycycline administration. Scale = 25 μm. Zoomed regions show HA-spastin expression in the crypt and villus. Scale = 10 μm. (C) Weights of control and Spastin^{Villi} mice on doxycycline-containing diet. Error bars show SD. (D, E) Microtubule organization in control and Spastin^{Villi} mice following doxycycline administration. Scale = 10 μm. (D) Top-down view. (E) Side view. (F) Quantification of α-tubulin intensity in control and Spastin^{Villi} cells. $n = 30$ cells from each of two mice for each genotype. Error bars show SD. (G) Quantification of HA-positive villar cells in Spastin^{Villi} mice. Six mice were examined, >190 cells/mouse. Error bars show SD. (H) Glu-tubulin staining in control and Spastin^{Villi} intestines. Scale = 10 μm. (I) Cross-section view of cell morphology upon spastin overexpression. White arrow indicates an inclusion body. Scale = 10 μm. (J) Quantification of cell heights in control and Spastin^{Villi} mice. $n = 90$ cells for each genotype. (K) Quantification of nuclear position in control and Spastin^{Villi} mice. $n = 75$ cells for each genotype. (L) Ezrin localization in control and Spastin^{Villi} mice. Scale = 20 μm. (M) Images and line scans of E-cadherin in control and Spastin^{Villi} mice. $n = 48$ junctions for each genotype. Scale = 10 μm. (N) ZO-1 localization in cross-sectional or top-down view in control and Spastin^{Villi} mice. Scale = 10 μm (top), 5 μm (bottom). **, $p < 0.01$; ***, $p < 0.001$.

Enterocytes in Spastin^{Villi} mice maintained their columnar shape. Spastin^{Villi} cells were slightly taller than controls, potentially due to distortions in the apical membrane (Figure 2, I–K). Microtubules have been implicated in the establishment and maintenance of cell polarity and in apical junctional complexes (Müsch, 2004; Meng *et al.*, 2008). However, we saw no defects in the polarization or intensity of either adherens junctions or tight junctions proteins in the mutant mice (Figure 2, M and N). Similarly, markers for apical transmembrane and peripheral membrane proteins remained polarized in the Spastin^{Villi} intestines (Figure 2L and Supplemental Figure 1D). Therefore, microtubules are not essential for the proper polarity and membrane localization of a number of key proteins. Notably, while we did not see an increase in basolateral staining of apical components, or the formation of lateral brush border-like structures, which were reported upon drug-induced microtubule depolymerization in intestinal explants, we did note the occasional presence of F-actin–rich structures within cells which appear similar to microvillar inclusions (Figure 2I). Notably, this system examines maintenance of polarity and not generation as we are disrupting microtubules in cells that are already polarized.

Although membrane polarity was largely unchanged in Spastin^{Villi} mice, the organization of the cytoplasm was significantly disrupted. Nuclei are normally highly aligned and localized at the base of enterocytes. In contrast, in Spastin^{Villi} mice, nuclei were misplaced along the apical–basal axis of the cells (Figure 2, I and K). This suggests that the microtubules prevent nuclear movement, either through steric exclusion or by providing tracks for basal movement. In addition to the nuclear positioning defects, the Golgi was also incorrectly placed and fragmented (Figure 3, A–C). By identifying small regions where spastin-expressing cells neighbored spastin-negative cells, we verified that the effects on nuclear position and Golgi placement were cell-autonomous (Figure 3D).

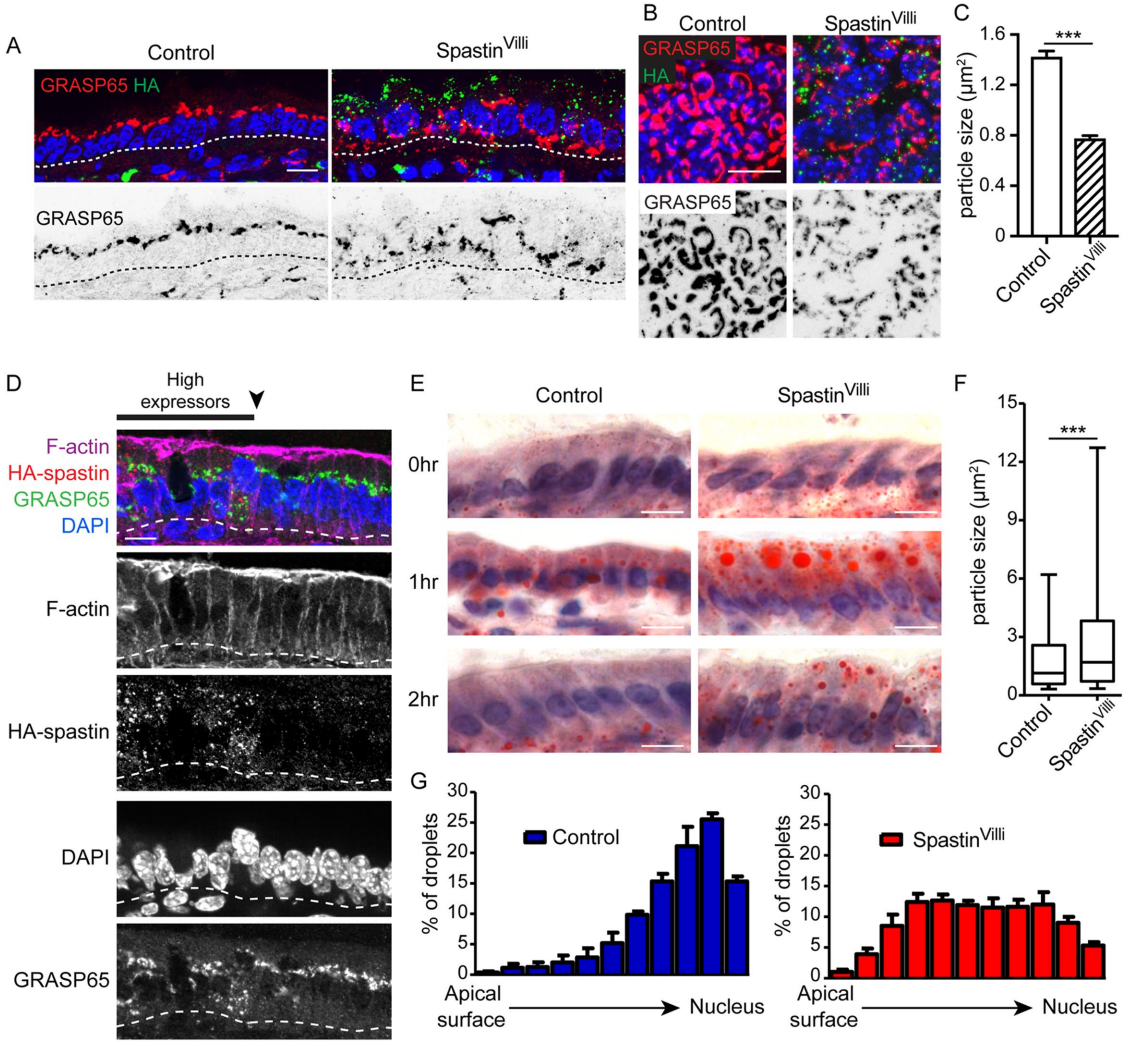

FIGURE 3: Microtubule disruption perturbs intracellular trafficking in the intestinal epithelium. (A) Cross-sectional view of GRASP65 localization in control or Spastin^{Villi} villar cells. Scale = 10 μm. (B) Top-down view of Golgi fragmentation in control and Spastin^{Villi} villi. Scale = 10 μm. (C) Quantification of Golgi particle size in control and Spastin^{Villi} mice. $n = 3$ mice for each genotype (2130 and 2899 particles for control and Spastin^{Villi} mice, respectively). (D) Golgi and nuclear positioning defects are cell-autonomous in the Spastin^{Villi} intestine. Scale = 10 μm. (E) Oil Red O staining of intestinal sections at indicated times following oil gavage. Scale = 10 μm. (F) Quantification of Oil Red O particle size in control and Spastin^{Villi} mice 1 h after oil gavage. $n = 3$ mice per genotype. Whiskers are the 5th to 95th percentile. (G) Quantification of lipid droplet intracellular placement in control and Spastin^{Villi} mice 1 h after oil gavage. $n > 650$ lipid droplets for each genotype. ***, $p < 0.001$.

The defects in cytoplasmic organization suggested that transport pathways for absorbed nutrients may also be affected. To directly test this, we gavaged mice with corn oil and examined their intestines at 1 and 2 h after treatment. Staining of the small intestine with Oil Red O revealed that oil was readily taken up by enterocytes in both control and Spastin^{Villi} intestine (Figure 3E). However, the oil was retained in large droplets in the Spastin^{Villi} intestines compared with controls. Lipid droplets were larger in size and preferentially localized to the apical region in mutant intestine (Figure 2F). Additionally, while oil trafficked through the cell in mice of both genotypes, the kinetics were delayed in Spastin^{Villi} enterocytes. In control mice, most of the oil was visible in the mesenchyme by 2 h, with little remaining in the epithelium. In contrast, substantial oil droplets remained in the mutant epithelium (Figure 2, E and G). Taken together, our data reveal that microtubules are required for proper lipid transport in the intestinal epithelium.

Analysis of microtubule disorganization due to loss of Nezha

To directly determine the similarities and differences between microtubule disorganization and microtubule loss, we generated a conditional (cKO) and global (KO) knockout allele of Nezha/CAMSAP3, which has previously been demonstrated to regulate microtubule organization in the intestine (Figure 4A and Supplemental Figure 2A; Toya *et al.*, 2016). We confirmed the loss of Nezha protein by Western blot analysis and immunofluorescence (Figure 4, B–D). Nezha has been reported to localize to the apical region of enterocytes in the villi, and we found that this localization was lost in

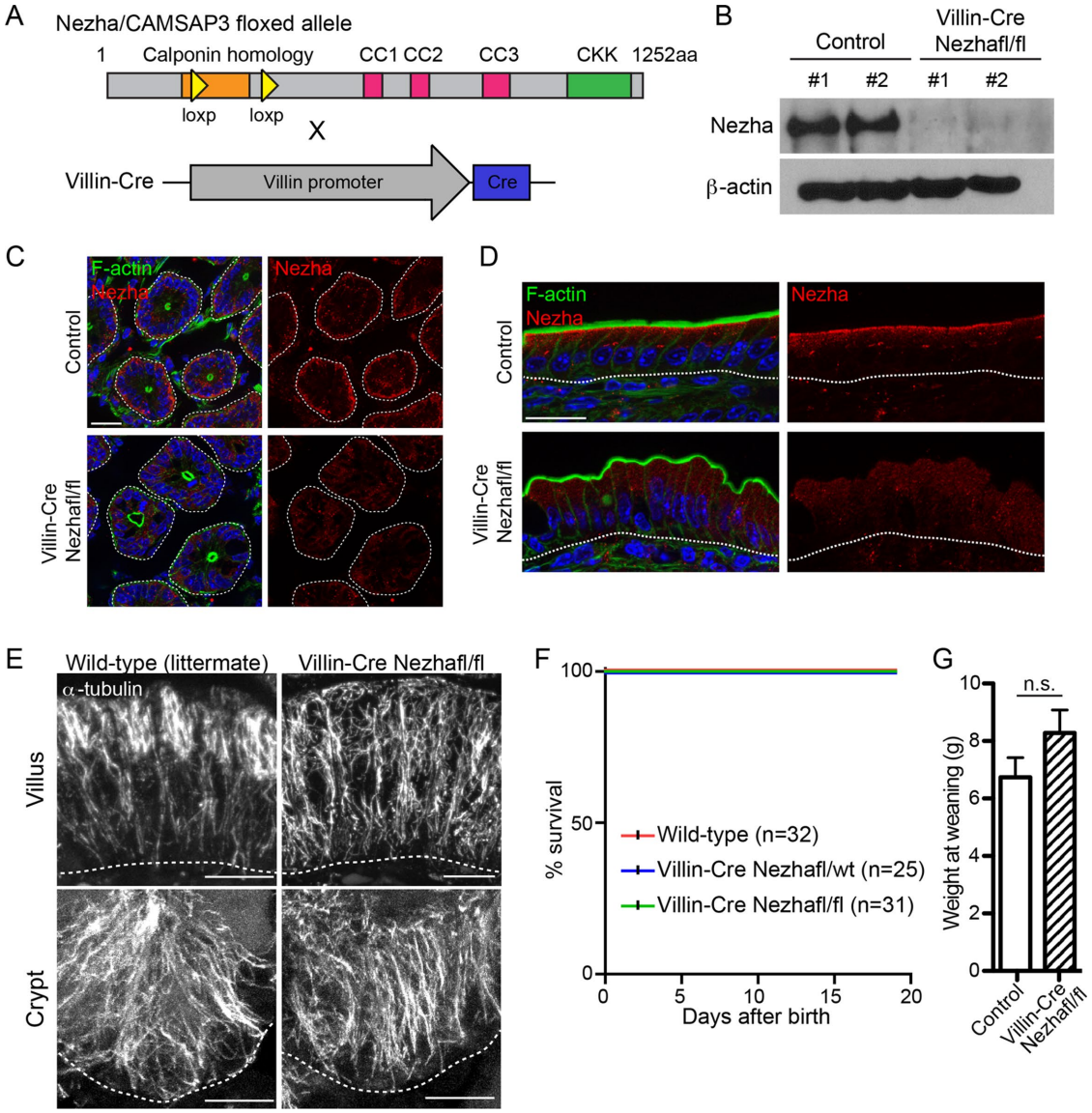

FIGURE 4: Characterization of intestine-specific Nezha/CAMSAP3 deletion in the intestinal epithelium. (A) Alleles used to generate Nezha/CAMSAP3 deletion in the intestinal epithelium. (B) Western blot showing Nezha depletion in Villin-Cre Nezhafl/fl intestinal epithelia. (C) Nezha staining in control and Villin-Cre Nezhafl/fl crypts. Scale = 20 μm. (D) Nezha staining in control and Villin-Cre Nezhafl/fl villi. Scale = 20 μm. (E) Microtubule organization in control and Villin-Cre Nezhafl/fl villar and crypt cells. Scale = 10 μm. (F) Kaplan-Meier plot of indicated genotypes. (G) Weights of indicated genotypes at weaning. n.s. = not significant.

the mutant mice. In crypts, Nezha was not enriched at the apical domain but, surprisingly, was found at the base of the cell. This was consistent with the basal network of microtubules that we observed specifically in crypts.

Previous work demonstrated that global loss of the CKK domain of Nezha resulted in failure to thrive and intestinal microtubule disorganization (Toya *et al.*, 2016). We similarly found that complete Nezha knockout mice were smaller from birth, with the majority of them succumbing within the first 2 wk of birth and a significant failure to gain weight. Few of these mice survived to adulthood (Supplemental Figure 2, B–D). This and previous work were consistent with the hypothesis that loss of Nezha function in the intestine led to the failure to thrive, but these data were inconsistent with our studies of the Spastin^{Villi} mice. To resolve this discrepancy, we generated conditional knockout mice in which Nezha was depleted in intestinal epithelial cells using the Villin-Cre transgenic line (el Marjou *et al.*, 2004). With this line Cre is expressed in both crypts and villi starting during embryogenesis. The growth of the conditional Nezha knockout mice was not impaired despite comparable microtubule disruption in the intestinal epithelia of Nezha cKO and KO mice (Figure 4, E–G). These data are consistent with our findings with the Spastin^{Villi} mice and reveal that microtubules in the differentiated cells of the intestinal epithelium are not essential for growth. They also indicate that the intestinal phenotypes caused by Nezha loss do not explain the lethality of global Nezha knockout mice and suggest that the requirement for Nezha resides within a different tissue.

Conditional loss of Nezha in the intestinal epithelium resulted in a disruption of microtubule organization, but microtubules were still present, and a significant number were still aligned along the apical–basal axis (Figure 4E). Despite this much less dramatic microtubule phenotype, the cell biological effects on cells were similar between Nezha loss and spastin overexpression. Of note, all observed intestinal phenotypes were identical between Nezha cKO and Nezha KO mice, despite the dramatic differences in their growth. Nuclei were displaced apically, and the Golgi apparatus and lysosomes had altered morphologies and localizations (Figure 5). As with the Spastin^{Villi} mice, adherens and tight junctions appeared normal (Supplemental Figure 3).

This work has demonstrated the effects of long-term loss of microtubules in the differentiated cells of the intestinal epithelium. Notably, as compared with differentiated epidermal cells, where microtubules play essential roles in cell shape, adhesion, morphogenesis, and differentiation, loss of microtubules had more subtle defects in the enterocytes. Notably, microtubule disruption and disorganization resulted in similar phenotypes. This suggests that gain-of-function effects, due to loss of polymer or increase of tubulin dimer, are not prominent in this tissue. The microtubules in enterocytes are important for cellular organization and lipid processing, but they are largely dispensable for enterocyte function under nutrient-rich conditions.

MATERIALS AND METHODS

Mouse lines and tissue

All mice were housed and maintained in accordance with Duke IACUC-approved protocols. Generation of TRE-HA-spastin mice was described previously (Muroyama and Lechler, 2017b). To generate the Nezha floxed allele, loxP sites were inserted flanking exons 5 and 9 of CAMSAP3. The Villin-rtTA mouse line was generated previously (Chen *et al.*, 2014). CMV-centrin-GFP mice were described previously (Higginbotham *et al.*, 2004). Villin-Cre and CMV-Cre mice were previously generated and were obtained from Jackson Laboratories (Schwenk *et al.*, 1995; el Marjou *et al.*, 2004).

Staining and antibodies

Intestinal tissue was either frozen in OCT and sectioned using a cryostat or used for epithelial wholemount isolation. To isolate the intestinal epithelium from the underlying mesenchyme, intestinal tissue was dissected and placed in Hank's balanced salt solution with 30 mM EDTA for 20 min at 37°C. Intestinal tissue was vigorously shaken to isolate the epithelium, and isolated epithelial sheets were fixed for downstream analysis. Depending on the primary antibody used, tissue samples were fixed with either 4% paraformaldehyde (PFA) at room temperature for 7 min or ice-cold methanol for 2 min. For microtubule fixation, intestines were fixed with glutaraldehyde fixation buffer (80 mM PIPES, pH 6.9, 50 mM NaCl, 2 mM $MgCl_2$, 0.4 mM $CaCl_2$, 1% glutaraldehyde, 3% PFA, 0.2% Triton-X) and then left to fix for 1 h. Tissue samples were then washed overnight at 4°C in phosphate-buffered saline (PBS) and subsequently incubated in 30% sucrose/PBS. Glutaraldehyde was quenched using sodium borohydride on tissue sections after a postfixation step. Slides were washed at least 3 × 30 min in PBS and then processed for staining.

The antibodies used in this study were rabbit anti-CDK5RAP2 (06-1398; EMD Millipore), rat anti–α-tubulin (sc-53029; Santa Cruz), rabbit anti-aPKC (9378S; Cell Signaling Technology), mouse anti-Nedd1 (39-J; Santa Cruz), rabbit anti–active caspase-3 (AF835; RandD systems), rat anti–β4 integrin (553745; BD Biosciences), rat anti-ECCD2 (kind gift from Colin Jamora, InStem, Bangalore, India), rabbit anti–ZO-1 (61-7300; Zymed/Invitrogen), rabbit anti-pericentrin (ab4448), rabbit anti-GRASP65 (ab30315), mouse anti-ezrin (ab4069), rabbit anti-Ki67 (ab15580; all from Abcam), mouse anti–γ-tubulin (clone GTU-88), mouse anti–β-actin (clone AC-15), rabbit anti-Nezha (SAB4200171), rabbit anti–α-catenin (C2081), rat anti-HA (11867423001; all from Sigma-Aldrich), mouse anti–aminopeptidase N (HBB3/156/63), rabbit anti-LAMP2 (ABL-93-s), and rat anti–keratin 8 (Troma-1; all from Developmental Studies Hybridoma Bank). F-actin was stained using fluorescently conjugated phalloidin (A12379, Invitrogen; and P1951, Sigma-Aldrich).

Image acquisition

Images of Nezha cKO and full KO intestines and some of the Spastin^{Villi} samples were acquired on a Zeiss Axio Imager microscope with Apotome attachment with the following objective lenses: 10× Plan-Neofluar 0.3 NA lens, 20× Plan-Apo 0.8 NA lens, 40× Plan-Neofluar 1.3 NA oil lens, and 63× Plan-Apo 1.4 NA oil lens. Images on the Axio Imager microscope were acquired using AxioVision software. Images for the remaining Spastin^{Villi} specimens were acquired using a Zeiss Axio Imager microscope with Apotome 2 attachment and Axiocam 506 mono camera with the same objectives. Images on this microscope were acquired using ZEN software. For fluorescence intensity comparisons between control and mutant tissues, images were always acquired within the same imaging session using the same exposure times and parameters.

Image quantification

All image quantification was performed using FIJI software. To quantify centrosomal CDK5RAP2 intensities along the crypt-villus axis, the mean pixel intensity of a 15 × 15 pixel box was measured around the centrosome. Three centrosomes were binned to create an average intensity for that location along the crypt-villus axis. Nuclear positions in Nezha KO and Spastin^{Villi} intestines were quantified by measuring the distance from the apical membrane (labeled by F-actin) and the top of the nucleus. For quantification of cortical α-catenin and ZO-1 intensity in Nezha KO intestines and E-cadherin intensity in Spastin^{Villi} intestines, line scans were performed in single

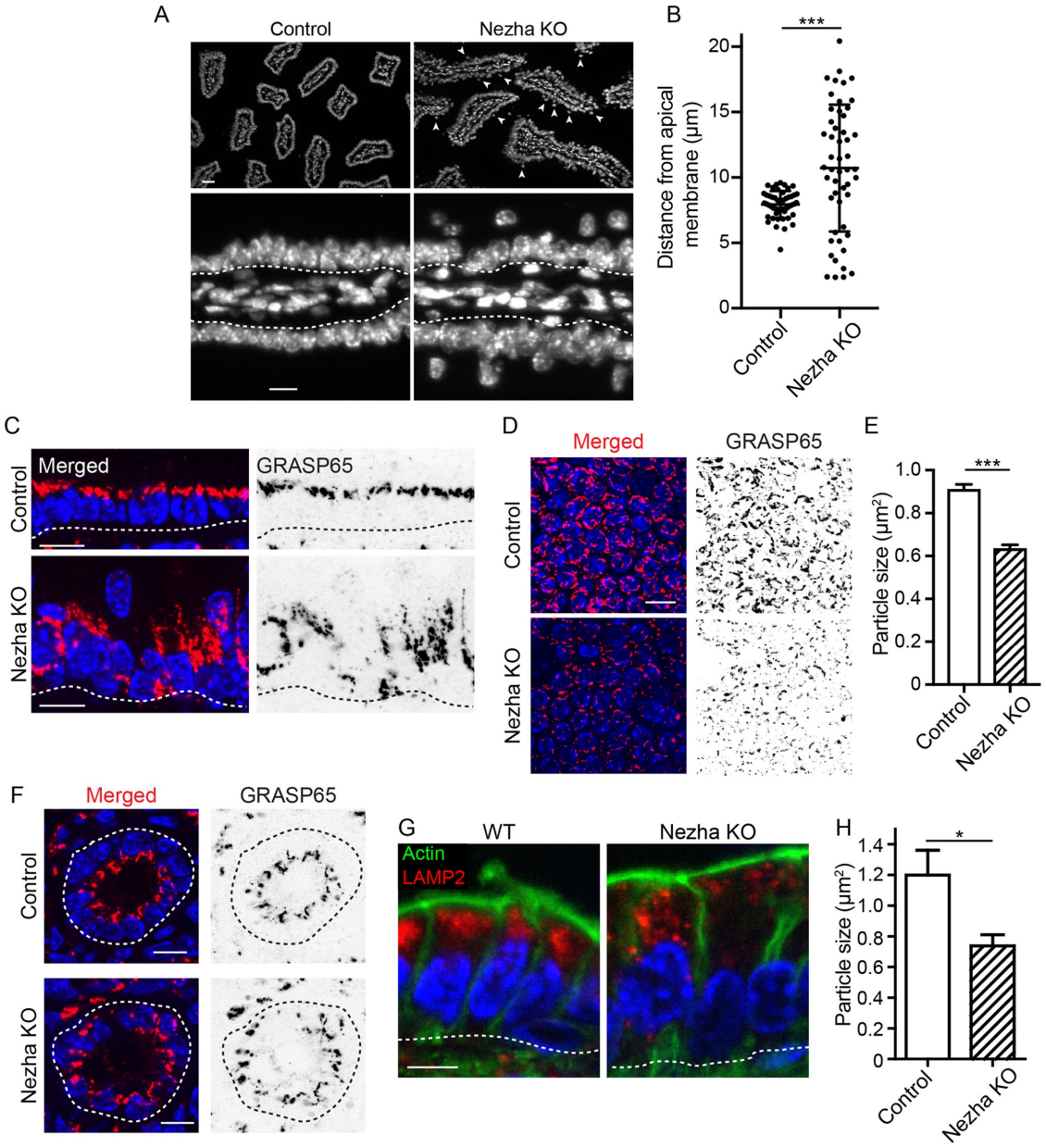

FIGURE 5: Organelle disorganization in the epithelium of the Nezha KO mouse. (A) Nuclear position in control and Nezha KO intestinal epithelia. Scale = 25 μm (top), 10 μm (bottom). (B) Quantification of nuclear position in control and Nezha KO cells. $n = 50$ and 51 cells for control and Spastin^{Villi} mice, respectively. Error bars show SD. (C) Cross-section view of GRASP65 localization in control and Nezha KO villar cells. Scale = 10 μm. (D) Top-down view of GRASP65 fragmentation in control and Nezha KO villar cells. Scale = 10 μm. (E) Quantification of Golgi particle size in control and Nezha KO villar cells. $n = 3$ mice for each genotype (2319 and 1213 total particles for control and Nezha KO mice, respectively). (F) GRASP65 localization in control and Nezha KO crypts. Scale = 10 μm. (G) LAMP2 localization in control and Nezha KO villi. Scale = 5 μm. (H) Quantification of LAMP2 particle size in control and Nezha KO cells. $n = 3$ mice for each genotype (one value for each mouse was calculated by averaging between 289 and 2159 particles per mouse). *, $p < 0.05$; ***, $p < 0.001$.

optical planes by manually drawing a 5-pixel-wide line across junctions. Fluorescence intensity along the line was calculated, and the maxima of each line were aligned. The ends were trimmed to normalize the line scans. To quantify centrosome position in villi, individual cells were outlined and the centroid was identified. Cells were normalized to 4 × 4 arbitrary units to account for differences in cell size and shape. Centrosomes were identified and then mapped onto the normalized coordinates relative to the centroid. To quantify GRASP65 particle size, a threshold was applied to images and all particles >0.1 μm^2 were quantified. To quantify LAMP2 particle size, thresholded single optical planes were subjected to particle analysis using FIJI. To quantify lipid droplets from Oil Red O stains, the red channel was thresholded. Line scans from the apical membrane to the nucleus were performed in individual cells and every point where the line crossed a lipid droplet was scored as a "1." If no lipid was encountered at that pixel, it was scored as a "0." Distribution of

the "1"s was then plotted over normalized distance to quantify the distribution of lipid droplets. For quantification of lipid droplet size, the same thresholded images were used. The epithelium was outlined and particle size was calculated using FIJI software. All statistical analyses were performed using GraphPad Prism 5 or 7 software. Unpaired Student's *t* tests were performed to determine significance. All error bars represent SEM unless otherwise noted in the figure legend.

Oil gavage assay

For the oil gavage experiments, control and Spastin^{Villi} mice were placed on doxycycline-containing food (VWR) for 48 h before the experiment. After 48 h, mice were fasted for 5 h and then gavaged with 50 µl of sterile-filtered corn oil. Mice were killed at 0, 1, and 2 h postgavage, and intestinal samples were frozen in OCT. For Oil Red O staining, intestinal sections on slides were fixed in 4% PFA for 7 min at room temperature, rinsed in ddH_2O, and then incubated with Oil Red O working solution (300 mg Oil Red O in 36% triethyl phosphate) for 30 min at room temperature. Slides were then washed with ddH_2O and stained with Mayer's hematoxylin and mounted.

ACKNOWLEDGMENTS

We thank the Duke Transgenic Core for generation of mice, Ben Stanger and Sylvia Robine for providing mouse strains, Julie Underwood for care of the mice, and members of the Lechler lab for comments on the manuscript. This work was supported by National Institutes of Health/National Institute of General Medical Sciences Grant no. R01GM111336 and National Institute of Arthritis and Musculoskeletal and Skin Diseases Grants no. R01AR055926 and no. R01AR067203 to T.L. and by a National Science Foundation graduate fellowship to A.M.

REFERENCES

Achler C, Filmer D, Merte C, Drenckhahn D (1989). Role of microtubules in polarized delivery of apical membrane proteins to the brush border of the intestinal epithelium. J Cell Biol 109, 179–189.

Bacallao R, Antony C, Dotti C, Karsenti E, Stelzer EH, Simons K (1989). The subcellular organization of Madin-Darby canine kidney cells during the formation of a polarized epithelium. J Cell Biol 109, 2817–2832.

Brodu V, Baffet AD, Le Droguen PM, Casanova J, Guichet A (2010). A developmentally regulated two-step process generates a noncentrosomal microtubule network in *Drosophila* tracheal cells. Dev Cell 18, 790–801.

Chen YJ, Finkbeiner SR, Weinblatt D, Emmett MJ, Tameire F, Yousefi M, Yang C, Maehr R, Zhou Q, Shemer R, *et al.* (2014). De novo formation of insulin-producing "neo-β cell islets" from intestinal crypts. Cell Rep 6, 1046–1058.

Clevers H (2013). The intestinal crypt, a prototype stem cell compartment. Cell 154, 274–284.

Cohen D, Brennwald PJ, Rodriguez-Boulan E, Musch A (2004). Mammalian PAR-1 determines epithelial lumen polarity by organizing the microtubule cytoskeleton. J Cell Biol 164, 717–727.

Eilers U, Klumperman J, Hauri HP (1989). Nocodazole, a microtubule-active drug, interferes with apical protein delivery in cultured intestinal epithelial cells (Caco-2). J Cell Biol 108, 13–22.

el Marjou F, Janssen KP, Chang BH, Li M, Hindie V, Chan L, Louvard D, Chambon P, Metzger D, Robine S (2004). Tissue-specific and inducible Cre-mediated recombination in the gut epithelium. Genesis 39, 186–193.

Feldman JL, Priess JR (2012). A role for the centrosome and PAR-3 in the hand-off of MTOC function during epithelial polarization. Curr Biol 22, 575–582.

Gilbert T, Le Bivic A, Quaroni A, Rodriguez-Boulan E (1991). Microtubular organization and its involvement in the biogenetic pathways of plasma membrane proteins in Caco-2 intestinal epithelial cells. J Cell Biol 113, 275–288.

Higginbotham H, Bielas S, Tanaka T, Gleeson JG (2004). Transgenic mouse line with green-fluorescent protein-labeled Centrin 2 allows visualization of the centrosome in living cells. Transgenic Res 13, 155–164.

Hugon JS, Bennett G, Pothier P, Ngoma Z (1987). Loss of microtubules and alteration of glycoprotein migration in organ cultures of mouse intestine exposed to nocodazole or colchicine. Cell Tissue Res 248, 653–662.

Matter K, Bucher K, Hauri HP (1990). Microtubule perturbation retards both the direct and the indirect apical pathway but does not affect sorting of plasma membrane proteins in intestinal epithelial cells (Caco-2). EMBO J 9, 3163–3170.

Meng W, Mushika Y, Ichii T, Takeichi M (2008). Anchorage of microtubule minus ends to adherens junctions regulates epithelial cell-cell contacts. Cell 135, 948–959.

Mogensen MM, Tucker JB, Stebbings H (1989). Microtubule polarities indicate that nucleation and capture of microtubules occurs at cell surfaces in *Drosophila*. J Cell Biol 108, 1445–1452.

Muroyama A, Lechler T (2017a). Microtubule organization, dynamics and functions in differentiated cells. Development 144, 3012–3021.

Muroyama A, Lechler T (2017b). A transgenic toolkit for visualizing and perturbing microtubules reveals unexpected functions in the epidermis. Elife 6, e29834.

Muroyama A, Seldin L, Lechler T (2016). Divergent regulation of functionally distinct γ-tubulin complexes during differentiation. J Cell Biol 213, 679–692.

Müsch A (2004). Microtubule organization and function in epithelial cells. Traffic 5, 1–9.

Noordstra I, Liu Q, Nijenhuis W, Hua S, Jiang K, Baars M, Remmelzwaal S, Martin M, Kapitein LC, Akhmanova A (2016). Control of apico–basal epithelial polarity by the microtubule minus-end-binding protein CAMSAP3 and spectraplakin ACF7. J Cell Sci 129, 4278–4288.

Quintin S, Wang S, Pontabry J, Bender A, Robin F, Hyenne V, Landmann F, Gally C, Oegema K, Labouesse M (2016). Non-centrosomal epidermal microtubules act in parallel to LET-502/ROCK to promote *C.elegans* elongation. Development 143, 160–173.

Reilein A, Yamada S, Nelson WJ (2005). Self-organization of an acentrosomal microtubule network at the basal cortex of polarized epithelial cells. J Cell Biol 171, 845–855.

Salas PJ (1999). Insoluble γ-tubulin-containing structures are anchored to the apical network of intermediate filaments in polarized CACO-2 epithelial cells. J Cell Biol 146, 645–658.

Salas PJ, Misek DE, Vega-Salas DE, Gundersen D, Cereijido M, Rodriguez-Boulan E (1986). Microtubules and actin filaments are not critically involved in the biogenesis of epithelial cell surface polarity. J Cell Biol 102, 1853–1867.

Schwenk F, Baron U, Rajewsky K (1995). A cre-transgenic mouse strain for the ubiquitous deletion of *loxP*-flanked gene segments including deletion in germ cells. Nucleic Acids Res 23, 5080–5081.

Sherwood NT, Sun Q, Xue M, Zhang B, Zinn K (2004). *Drosophila* spastin regulates synaptic microtubule networks and is required for normal motor function. PLoS Biol 2, e429.

Tan DW, Barker N (2014). Intestinal stem cells and their defining niche. Curr Top Dev Biol 107, 77–107.

Toya M, Kobayashi S, Kawasaki M, Shioi G, Kaneko M, Ishiuchi T, Misaki K, Meng W, Takeichi M (2016). CAMSAP3 orients the apical-to-basal polarity of microtubule arrays in epithelial cells. Proc Natl Acad Sci USA 113, 332–337.

Toya M, Takeichi M (2016). Organization of non-centrosomal microtubules in epithelial cells. Cell Struct Funct 41, 127–135.

Troutt LL, Burnside B (1988). The unusual microtubule polarity in teleost retinal pigment epithelial cells. J Cell Biol 107, 1461–1464.

Valenstein ML, Roll-Mecak A (2016). Graded control of microtubule severing by tubulin glutamylation. Cell 164, 911–921.

Yano T, Matsui T, Tamura A, Uji M, Tsukita S (2013). The association of microtubules with tight junctions is promoted by cingulin phosphorylation by AMPK. J Cell Biol 203, 605–614.